

N94-15559

THE PRECISION OF TODAY'S SATELLITE LASER RANGING SYSTEMS

P.J.Dunn and M.H.Torrence, Hughes STX Corp., Lanham,MD
V.Hussen, Bendix Field Engineering Corporation, Greenbelt,MD
M.Pearlman, Smithsonian Astrophysical Observatory, Cambridge,Mass

Introduction

Recent improvements in the accuracy of modern SLR systems are strengthened by the new capability of many instruments to track an increasing number of geodetic satellite targets without significant scheduling conflict. This will allow the refinement of some geophysical parameters, such as solid Earth tidal effects and GM, and the improved temporal resolution of others, such as Earth orientation and station position. Better time resolution for the locations of fixed observatories will allow us to monitor more subtle motions at the stations, and transportable systems will be able to provide indicators of long term trends with shorter occupations. If we are to take advantage of these improvements, care must be taken to preserve the essential accuracy of an increasing volume of range observations at each stage of the data reduction process.

The Range Measurement

The SLR measurement is computed as one half of the product of an adopted value of the speed of light and the observed interval between the transmit time of the pulse and the time of a detected return. The essential simplicity of this process is tempered by the need for careful calibration for system delay and atmospheric refraction, as well as for an accurate survey of mount eccentricity and other important local coordinates to match the millimeter accuracy of the best current systems. The influence of satellite signature and detector time-walk must also be considered at this high accuracy level, and we consider here the particular need to preserve any details of these effects which may be lost in the current normal point compression process.

Normal Point Generation

The loss of detail at each stage of the process to reduce engineering data to normal points is illustrated in Table 1, which shows the information content of each of the parameters measured by most instruments for a typical satellite pass or pass sequence. Information on receive energy level is not necessary if all time-walk characteristics of the detector system have been eliminated or corrected before data compression. Neither will the absence of calibration details matter if the distribution of returns is identical to that from the satellite and the same algorithm is applied to reduce each observation. The accuracy of the satellite observations will be preserved as long as the return distribution is normal (or Gaussian) about the mean range.

Shape Factors

Two measures of the deviation of a distribution from normal are illustrated in Figure 1. Any skewness in the pattern of range residuals about the mean would bias normal points if we assume that the peak of the distribution is a better measure of the range. Skewness is computed from the third moment of the residual distribution, just as the standard deviation is based on the second moment: it is positive for a distribution with a tail towards long ranges, and negative (a rare

occurrence) when the noise is short. Another shape factor can be simply obtained as a combination of third and fourth moments: kurtosis gives an indication of flatness (low values) or peakiness (high values). A residual histogram with low kurtosis values can be produced by using a lower value of the sigma multiplier than three for data editing (clipping); high kurtosis values are obtained when a larger sigma multiplier than three is employed, and the return signal appears as a spike in the background noise.

Interpretative Aids

The utility of these shape factors can be demonstrated with examples from several different systems. To illustrate the mechanism used to build the basic contour picture which we have adopted for data quality assurance we refer to Figure 2, which is a three-dimensional accumulation of a number of pass histograms for LAGEOS ranges taken at the Grasse Observatory during a three month interval. The vertical scale shows the percentage of range measurements which lie within ten millimeter bins distributed about the mean value. An imaginative reader will observe a progression from a nearly symmetrical distribution in December 1990 to a significantly skewed pattern in February 1991: the front profile on 91-02-27 demonstrates the characteristic of long noise. The coarse grain caused by the centimeter bin width is softened in the contour of the same data which is shown in Figure 3. The grey band of the contour scale shows a shift in the distribution in early January 1991 and the lighter peaks also suggest a change in character at this time: the darker contour levels emphasize the asymmetrical tail towards long ranges in January and February 1991.

Quantifying the residual behavior

Numerical descriptors for the changing residual pattern are shown in the scatter plot to the left of the contour frame. The crosses depict a normalized skew factor which jumps from a low (moderately skewed) to a high value at the same time that a low (flat peak) kurtosis measure returns to a nominal level as shown by the open circles. The change in the pattern was caused by a relaxation of the tight data editing criterion applied to the earlier observations which clipped the distribution and muted the intrinsic asymmetry exposed with more liberal editing. The standard deviation of the full-rate data is recorded with the normal points in the currently adopted compression scheme, so this event would be flagged as an increase in noise level, but the skew and kurtosis shape factors provide improved diagnostics at a relatively low computational cost.

The cause of any data asymmetry can be isolated by inspecting the distribution of the calibration measurements: if the asymmetry is restricted to the satellite returns, the shift in the effective range measurement due to the editing change would amount to over a centimeter and would cause an even larger change in the apparent height of a station position determined from these observations. On the other hand, similar levels of asymmetry in the ground target returns would suggest a source in the detector rather than the satellite, and if the same editing scheme was used for each data type, there would be no bias in the satellite measurements.

Satellite and Calibration Target Data

We have considered the shape of distributions from calibration and satellite targets in an analysis of observations from six GSFC systems collected in early 1992. Figure 4 shows a collage of residual histogram contours from the systems tracking several different satellites: ERS-1(E), Starlette(S), LAGEOS(L), Ajisal(A), ETALON-1(E1), and ETALON-2(E2). This broad representation shows at a glance the higher noise level of the ETALON satellite returns, as well as the tight

precision of data from lower-orbiting satellites like ERS-1, which amounts to about 5 millimeters for MOBILAS-7. The same ten millimeter bin scale is used to describe the characteristics of these instruments as for the data from Grasse in the earlier example.

The patterns for the appropriate calibration passes are given in Figure 5: they show less variation than the satellite data, and allow us to discriminate satellite-dependent variations from detector characteristics. None of the systems depicted here shows a systematic bias of more than a millimeter, but subtle effects in the distribution for an individual system can be detected and quantified by the skew and kurtosis shape factors plotted in the Figures provided for a couple of the instruments. The satellite returns for Moblas-7 show no consistent kurtosis but a hint of the positive skew typical of all systems' observations of the ETALON satellites (at the bottom of the plot); the MOBILAS-7 calibration returns are slightly clipped (low kurtosis). On the other hand, TLRS-4's satellite returns show no significant skew, but indicate a hint of clipping; this instrument's calibration data possesses the rare property of slight negative skewness.

Summary

The effects of these idiosyncrasies in residual pattern for the GSFC systems is well below the accuracy threshold for any currently employed application of the data, but they could be used to characterize subtle changes in system characteristics. We have attempted to demonstrate in the above examples the enhanced ability to monitor data quality for any SLR system with some simple shape factors which can be computed economically in the normal point compression stage. Regular inspection of these parameters can flag changes in data characteristics which affect range accuracy, and also provide reassurance that our most advanced systems do indeed attain the millimeter accuracy of which they are capable.

| LEVEL | DATA TYPE | GRANULARITY | | |
|-------|---------------------|-------------|----------------|-------------|
| | | ROUNDTrip | RECEIVE ENERGY | MET. |
| | | SAT. CAL. | SAT. CAL. | |
| 0 | RAW ENGINEERING | POINT POINT | POINT POINT | POINT POINT |
| 1a | PROCESSED FULL RATE | POINT PASS | POINT | POINT |
| 1b | NORMAL POINTS | BIN PASS | | BIN |

TABLE 1: The information content of each data type is diluted in each step of the data compression process, although some statistical properties of the original distribution are recorded.

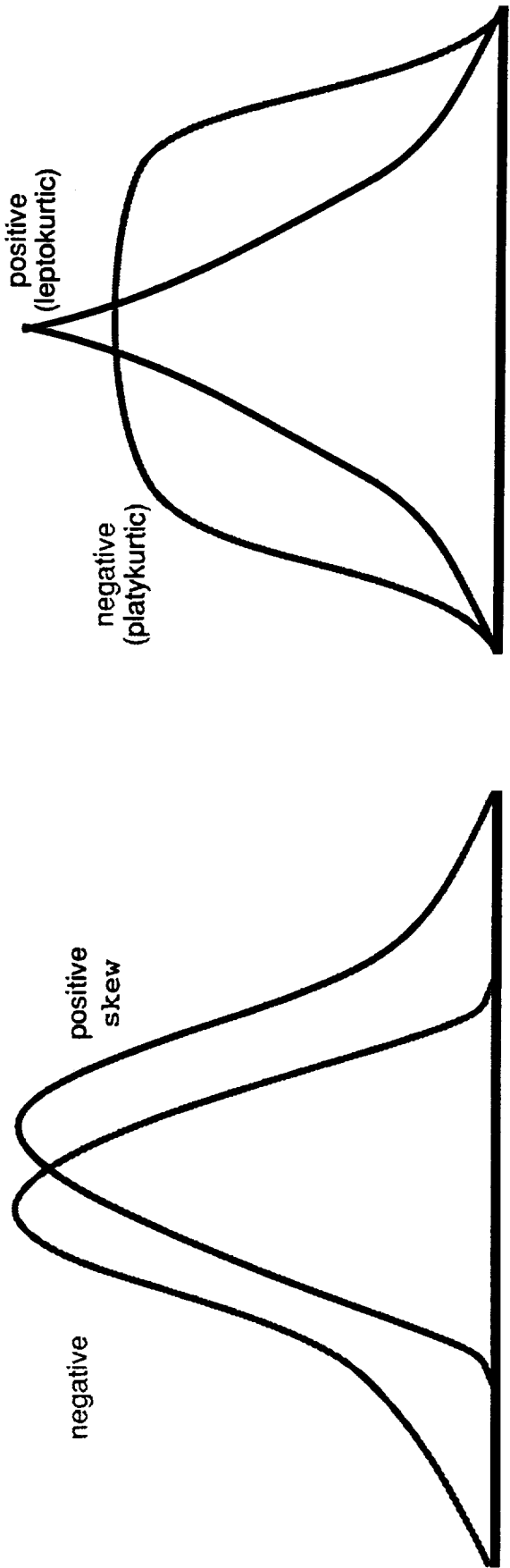


FIGURE 1: Shape factors which characterize the range deviation from normal can be used to supplement the root mean square value which is usually recorded. Slight positive skew is observed in almost all the systems; negative kurtosis (compared to a normal value of 3.0) is seen when a low editing multiplier (<3) "clips" the distribution and positive kurtosis is a symptom of loose editing (>3) which does not reject background noise.

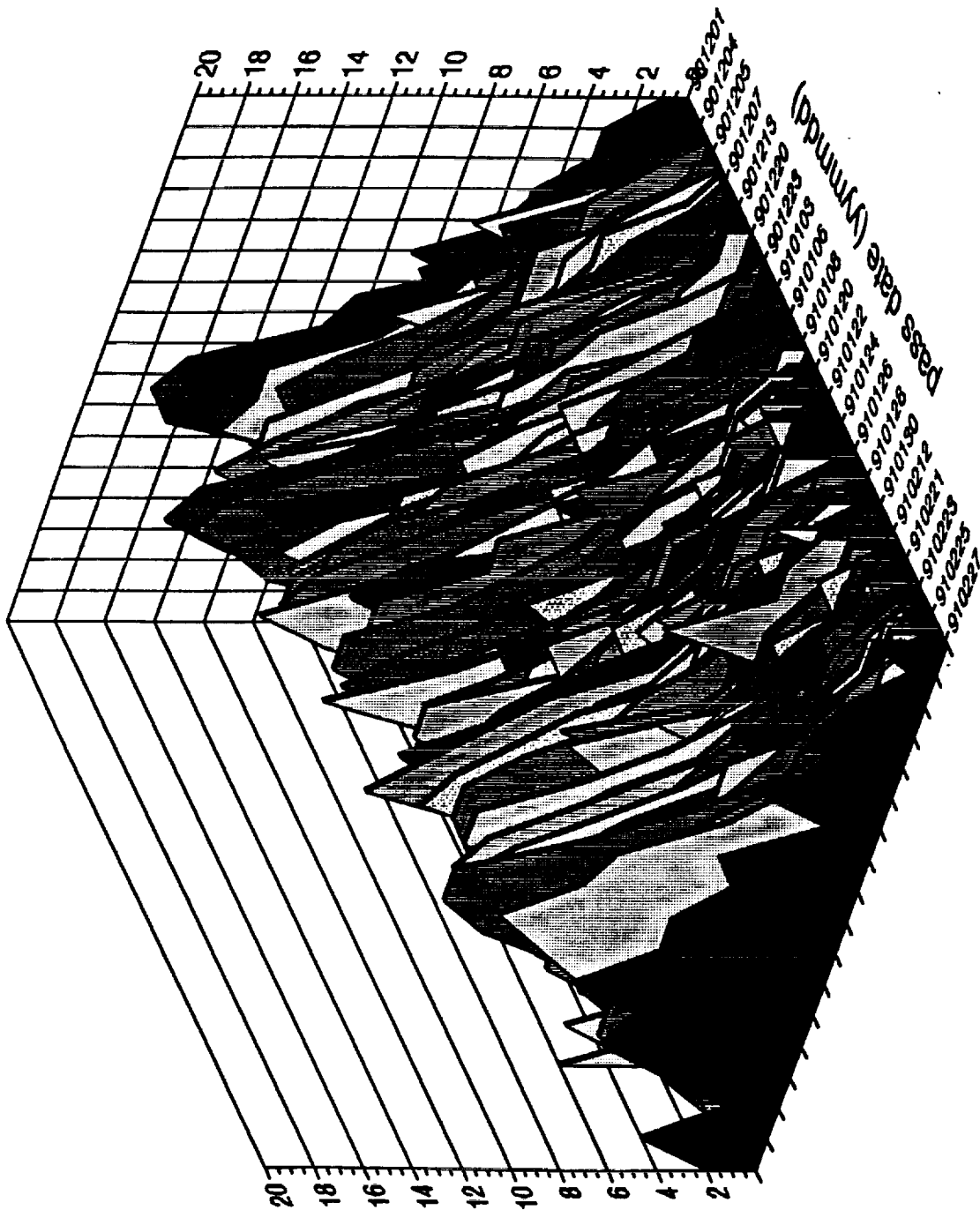


FIGURE 2: The build-up of pass histograms shows a progression towards a skewed distribution with time for LAGEOS data from the Grasse Observatory. The horizontal scale bin width is ten millimeters, and the ordinate gives the percentage of observations within each bin.

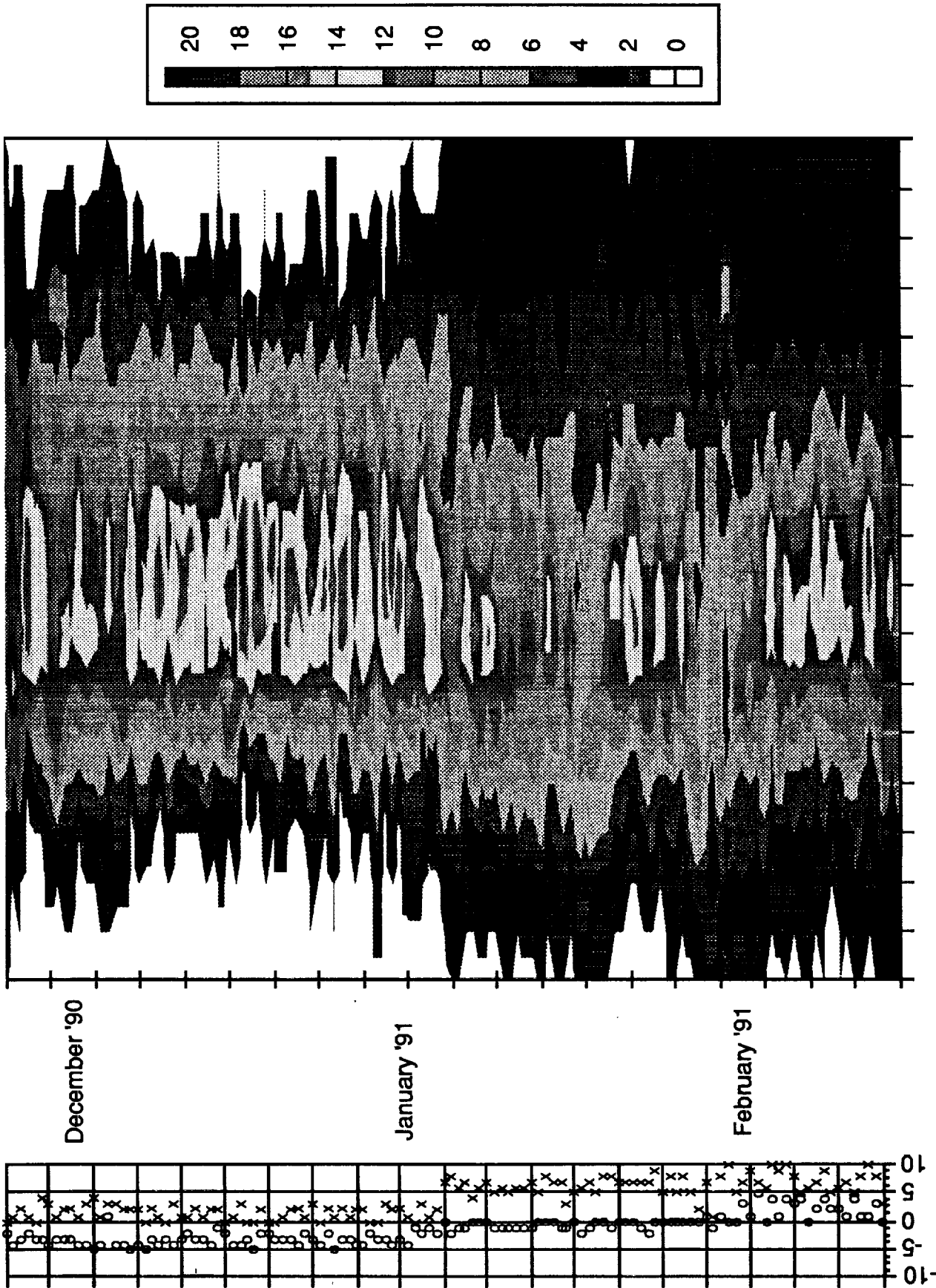


Figure 3. Pass-by-pass 10 mm binned LAGEOS residuals from Grasse.

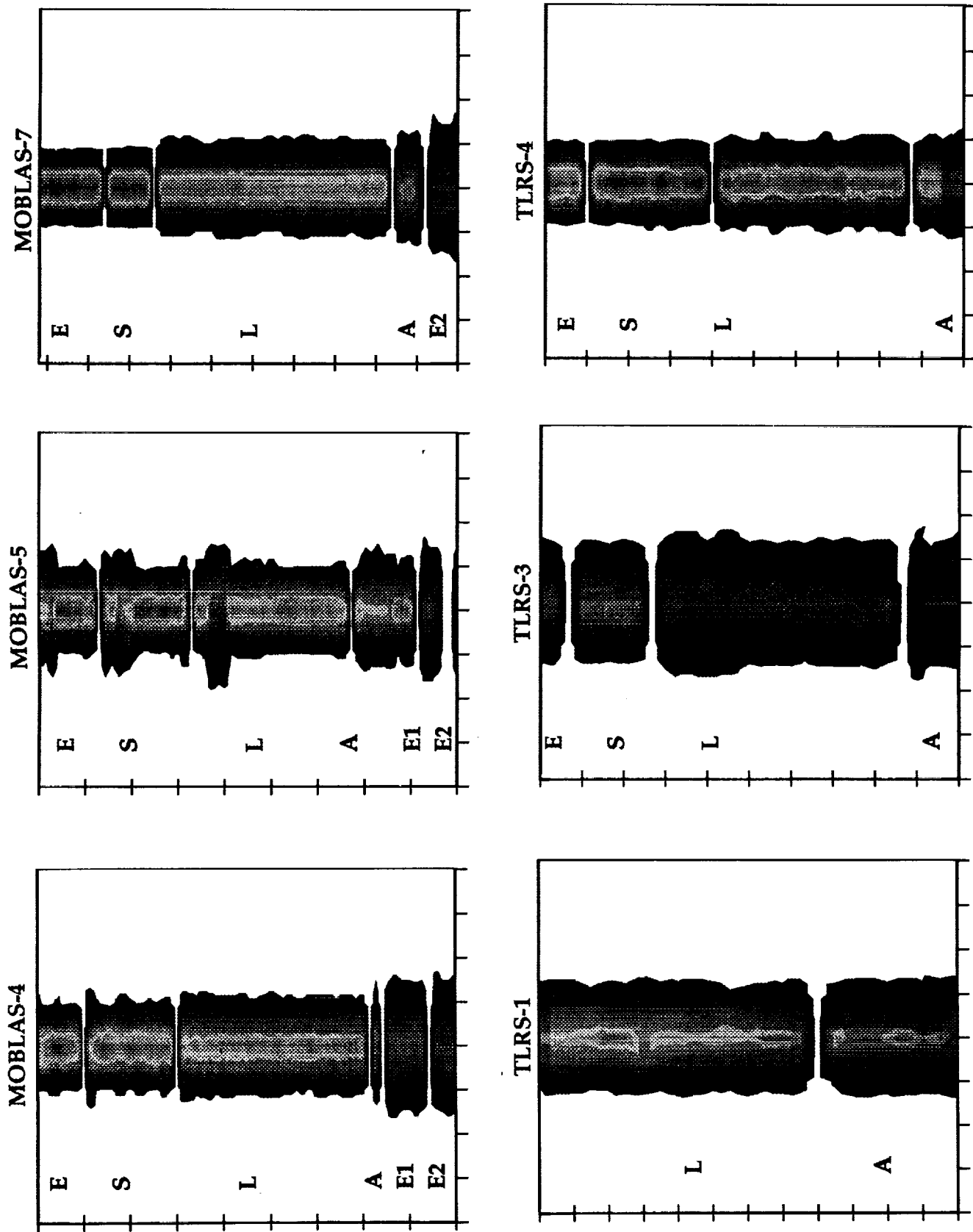


Figure 4. Satellite binned residuals.

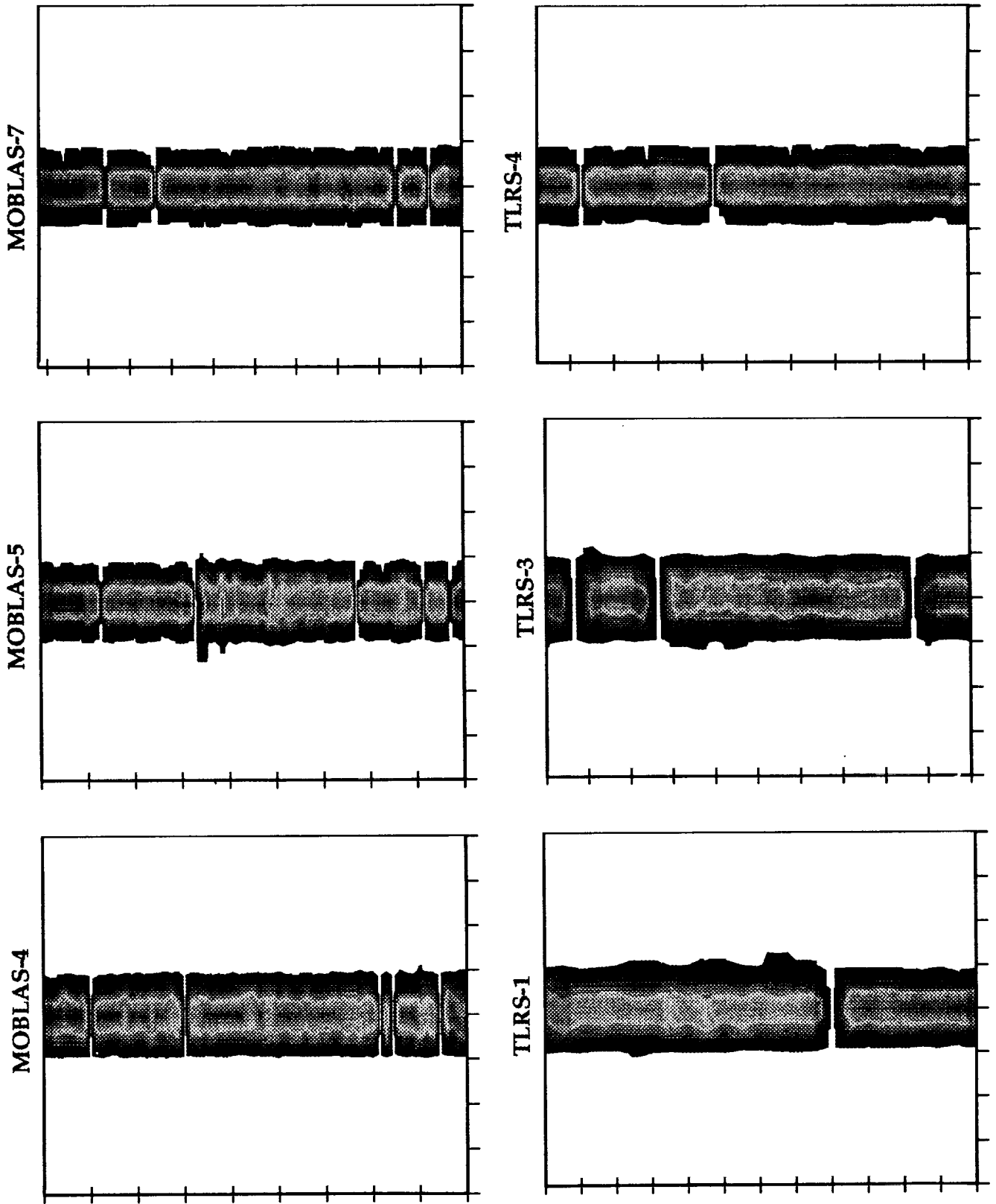


Figure 5. Calibration binned residuals

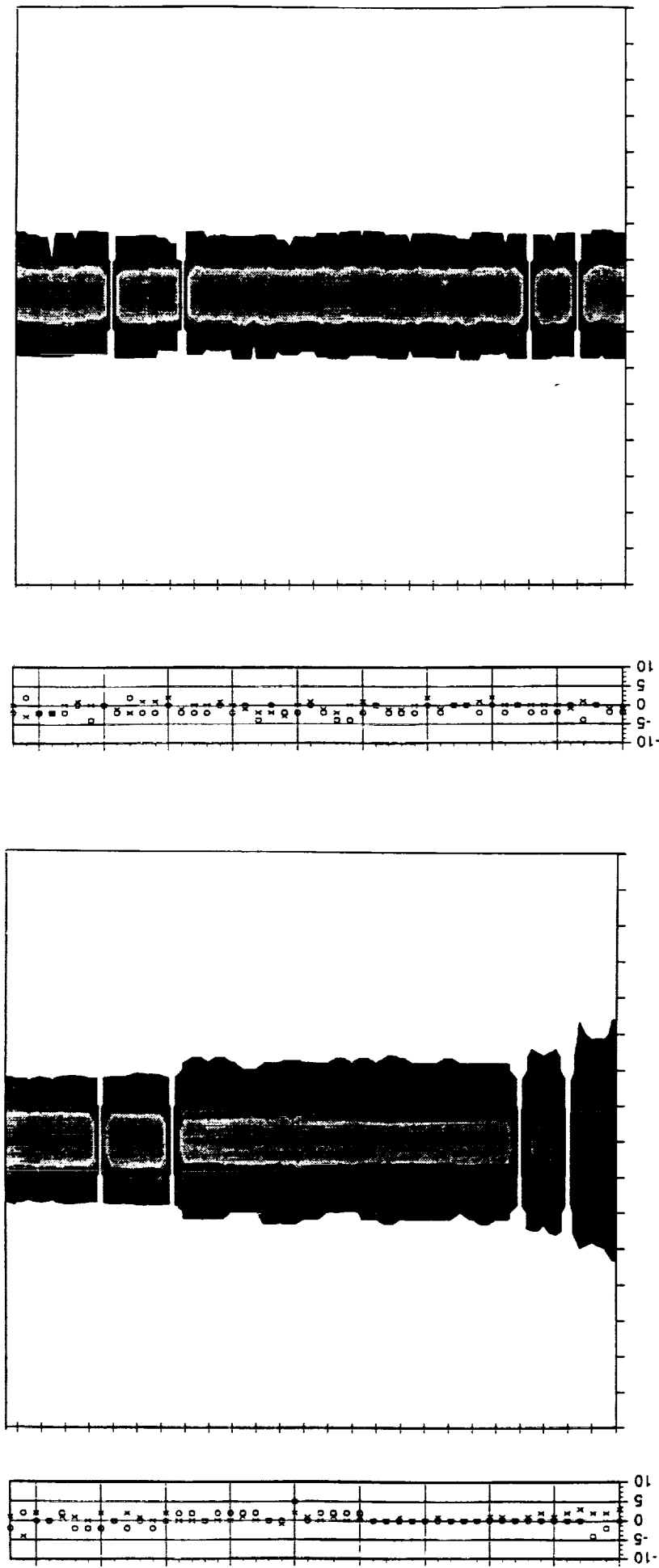


Figure 6a. Satellite and calibration binned residuals from MOBLAS-7

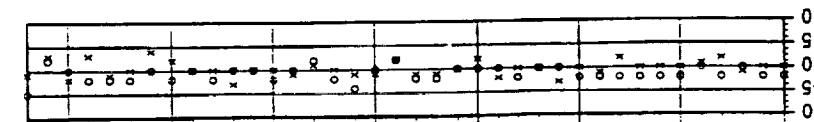
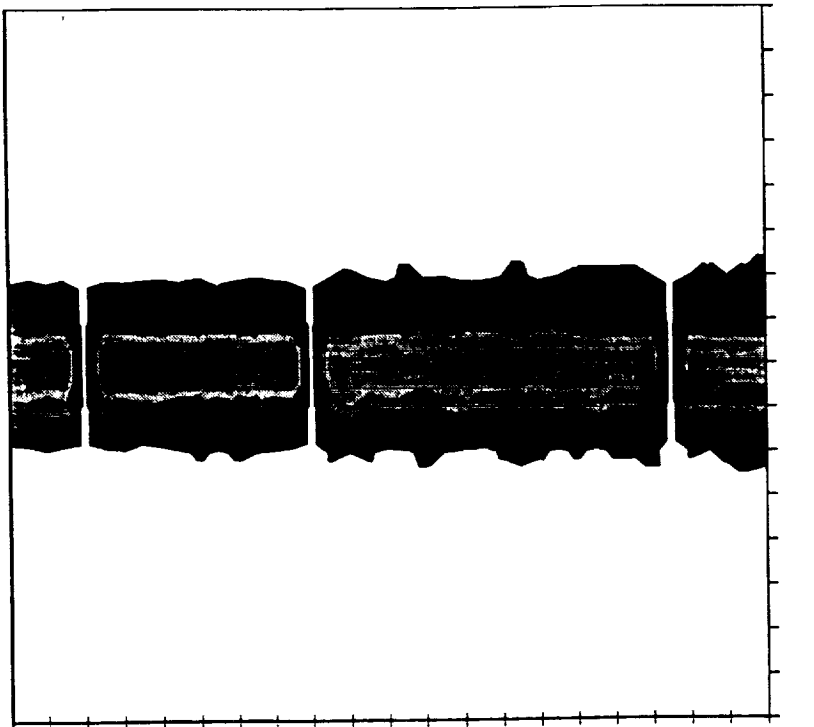
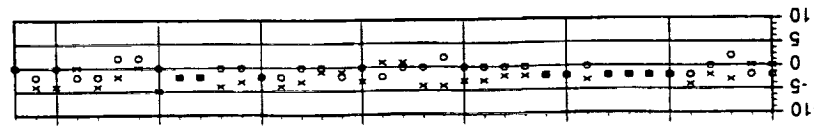
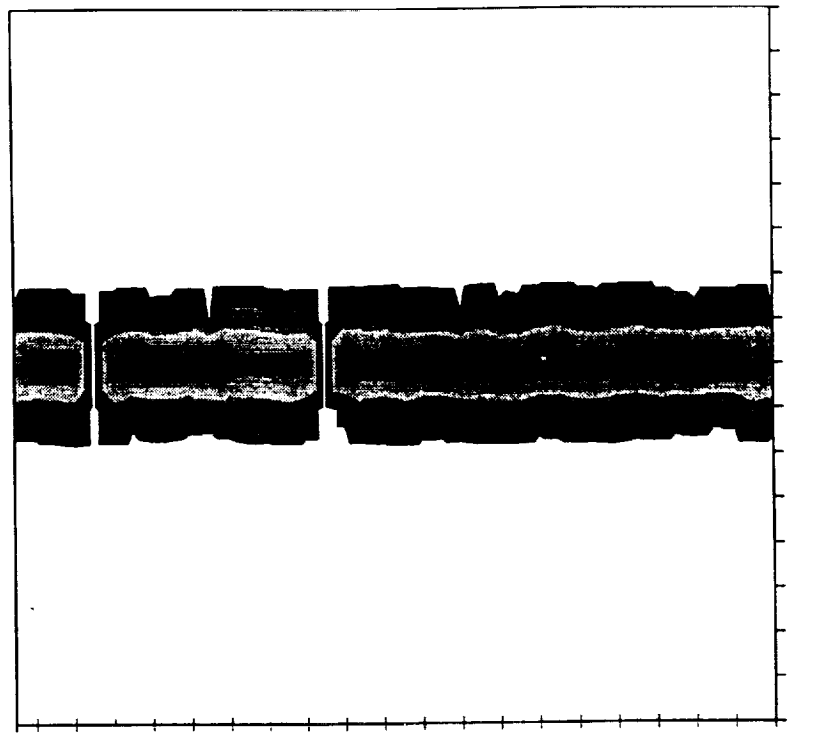


Figure 6b. Satellite and calibration binned residuals from TLRs-4.